IOP PUBLISHING PLASMA PHYSICS AND CONTROLLED FUSION

Plasma Phys. Control. Fusion **50** (2008) 074013 (11pp) doi:10.1088/0741-3335/50/7/074013

Simulations of a plasmoid penetrating a magnetic barrier

H Gunell[1], T Hurtig[2], H Nilsson[3], M Koepke[1,4] and N Brenning[4]

[1] Department of Physics, West Virginia University, Morgantown, WV 26506-6315, USA
[2] Swedish Defence Research Agency, Grindsjön Research Centre, SE-147 25 Tumba, Sweden
[3] Swedish Institute of Space Physics, PO Box 812, SE-981 28 Kiruna, Sweden
[4] Division of Space and Plasma Physics, School of Electrical Engineering, Royal Institute of Technology, SE-100 44 Stockholm, Sweden

E-mail: herbert.gunell@physics.org

Received 26 October 2007, in final form 19 March 2008
Published 4 June 2008
Online at stacks.iop.org/PPCF/50/074013

Abstract

Plasma structures, here typified by the term 'plasmoids', in the solar wind impacting on the magnetopause, i.e. the boundary between the solar wind and the Earth's magnetosphere, can penetrate this boundary and be injected into the magnetosphere. This can happen either by expulsion of the magnetic field from the structure and subsequent diffusion of the magnetic field into the structure or by the formation of a polarization electric field that lets the plasma structure $\boldsymbol{E} \times \boldsymbol{B}$-drift into the earth's magnetic field. In both cases a collisionless resistivity is required at some stage of the process. While magnetic expulsion requires electromagnetic models for its description, polarization can be modelled electrostatically and both processes can be, and have been, studied in laboratory experiments.

We present three-dimensional electrostatic particle-in-cell simulations that reproduce large-amplitude waves, in the lower-hybrid range, that have been observed in laboratory experiments. Lower-hybrid waves have also been seen at the magnetopause of the earth. We consider the implications for spacecraft-based studies of magnetopause penetration, and suggest that the search for penetrating plasma structures should emphasize cases in which the interplanetary magnetic field is oriented northwards, as this configuration is less likely for reconnection. The application of theoretical predictions to the magnetopause environment shows that a plasma structure penetrating via polarization needs to be small, i.e. less than 10–100 km wide for typical parameters, and that wave processes at the magnetopause are needed to create such small structures. A larger structure can penetrate by means of magnetic expulsion.

(Some figures in this article are in colour only in the electronic version)

1. Introduction

In the late 1970s Lemaire suggested that inhomogeneities in the solar wind can penetrate the magnetopause as plasma filaments through a process called impulsive penetration [1]. Rocket [2] and satellite [3, 4] based measurements have shown evidence of magnetosheath plasma inside the magnetosphere. In the laboratory, similar cross field transport has been studied by letting a flowing plasma both impact and penetrate a magnetic barrier [5–8].

Impulsive penetration has been studied numerically in one and two dimensions using ideal, resistive and Hall MHD and particle-in-cell and hybrid simulations. A review of these can be found in [9]. More recently two-dimensional Vlasov simulations [10] and two-dimensional [8] and three-dimensional [11] electrostatic particle-in-cell simulations have been published.

As a plasmoid enters a transverse magnetic field, ions and electrons gyrate in opposite directions and, thereby, a polarization electric field $\boldsymbol{E} = -\boldsymbol{v} \times \boldsymbol{B}$ is set up, which will enable the plasma to continue moving with its initial velocity by means of an $\boldsymbol{E} \times \boldsymbol{B}$-drift. The energy of the electric field must come from the kinetic energy of the plasma and theoretical results predicted that the condition $W_\mathrm{K} \gg W_\mathrm{E}$ is required for penetration via self-polarization, where $W_\mathrm{K} = \frac{1}{2} n_0 m_\mathrm{i} v_0^2$ is the kinetic energy density of the plasma and $W_\mathrm{E} = \frac{1}{2}\epsilon_0 (v_0 B_\perp)^2$ is the energy density of the polarization electric field [12]. Here n_0 is the plasma density, m_i the ion mass and $\boldsymbol{v}_0$ the bulk velocity of the plasma. It was later shown that, for quasi-neutrality to be maintained, $W_\mathrm{K}/W_\mathrm{E} \gg \sqrt{m_\mathrm{i}/m_\mathrm{e}}$ is required [13]. It was found experimentally that unless $W_\mathrm{K}/W_\mathrm{E} > 10\sqrt{m_\mathrm{i}/m_\mathrm{e}}$, penetration is prevented [6]. A recent series of experiments revealed lower-hybrid wave-driven electron transport perpendicular to both $\boldsymbol{B}$ and $\boldsymbol{v}_0$ [7, 8]. These experiments have been modelled using particle-in-cell simulations [8, 11]. Lower-hybrid waves have also been observed at the magnetopause by the Cluster spacecraft [14].

Brenning *et al* [15] suggested an analytical model for the non-linear magnetic diffusion, and proposed that experiments and observations can be classified by dividing the parameter space into three regions corresponding to three different outcomes of a penetration experiment. This parameter space is spanned by the kinetic beta $\beta_\mathrm{k} = W_\mathrm{K}/W_\mathrm{B}$, and the quantity

$$\Pi = \frac{w}{r_\mathrm{gi}} K \sqrt{\beta_\mathrm{ith}}, \tag{1}$$

which we shall call the penetrability parameter. Here w is the width of the plasmoid, $r_\mathrm{gi} = m_\mathrm{i} v_0/(\mathrm{e}B_\perp)$ the ion gyro-radius, $W_\mathrm{B} = B_\perp^2/(2\mu_0)$ the magnetic energy, $\beta_\mathrm{ith} = \frac{1}{2} n_0 m_\mathrm{i} v_\mathrm{ith}^2 / W_\mathrm{B}$ the ion thermal beta and $K = 2.3$ is an empirically determined constant. The three regions are [15]

(i) *Expulsion.* A plasma structure can penetrate a magnetic barrier by expelling the magnetic field if $\beta_\mathrm{k} > 1$ and $\Pi > 1/\sqrt{\beta_\mathrm{k}}$.
(ii) *Self-polarization.* A plasma structure can penetrate a magnetic barrier by convection in a polarization electric field if $\Pi < \sqrt{\beta_\mathrm{k}}$ for $\beta_\mathrm{k} < 1$ and $\Pi < 1/\sqrt{\beta_\mathrm{k}}$ for $\beta_\mathrm{k} > 1$.
(iii) *Rejection.* The plasma cannot penetrate the magnetic barrier if $\beta_\mathrm{k} < 1$ and $\Pi > \sqrt{\beta_\mathrm{k}}$.

The requirements on computer simulations are quite different in different regions of $\beta_\mathrm{k} - \Pi$ space. While, for example, electrostatic particle-in-cell simulations can be used to model the self-polarization regime, electromagnetic simulations are required to model the expulsion regime. Higher values of the penetrability parameter are associated with either a larger plasmoid width or a smaller gyro-radius, both of which demand a higher number of grid points. Similarly, the requirements on laboratory experiments are quite different in the different

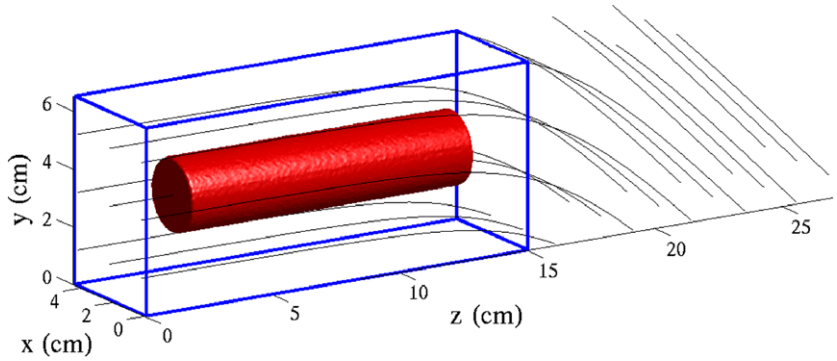

Figure 1. Schematic of the simulation setup showing the simulation box, the initial plasma and the magnetic field configuration.

parameter regimes. To verify the inequalities and to gain a more complete understanding of the impulsive penetration process, one would need to conduct a series of laboratory and computer experiments, where all three regions of $\beta_k - \Pi$ space are sampled and the boundaries between them are studied in some detail.

The boundary between the expulsion and self-polarization regimes is gradual and was studied experimentally in [15]. In this paper, we extend the three-dimensional particle-in-cell simulations of Hurtig *et al* [11] and present the results of two simulation cases in the self-polarization regime. We show that waves in the lower-hybrid frequency range appear in this regime and how the difference in density between the two cases influence the wave properties and penetrability. Like the previous simulations [11], the simulations presented here are primarily designed to model the laboratory experiments. We discuss the implications the results have for studies of the penetration process at the magnetopause, and the applicability of different theoretical models to the laboratory and space situations.

2. Simulation model

We have used a three-dimensional electrostatic particle-in-cell code with a moving grid and open boundaries [11]. The use of open boundary conditions means that when the charge of the particles has been assigned to the grid an extra step is inserted where the potential on the boundaries of the simulation box is calculated under the assumption that the space between these boundaries and infinity is empty. Poisson's equation is then solved using this potential as a Dirichlet boundary condition. The moving grid makes the computations more efficient by allowing us to solve Poisson's equation only in the region near the plasma cylinder and not in the empty space in front of and behind it.

A schematic of the simulation geometry is shown in figure 1. We simulate a cylindrical plasma with initial density n_0 moving with initial velocity $\boldsymbol{v}_0$ in the z-direction. The simulation box also moves with the same velocity. At the start of the simulation, the plasma coexists with a horizontal magnetic field. The travelling plasmoid passes through a transition region and enters a region characterized by a magnetic field that is directed at a 45° angle from the horizontal. The magnetic field is given by

$$\boldsymbol{B} = B_0 \left(\left(\frac{1}{1 + \mathrm{e}^{(z - z_\mathrm{T})/\delta}} - 1 \right) \hat{y} + \hat{z} \right), \tag{2}$$

Table 1. Parameters at the magnetopause region [14, 16], the two simulations presented here, and the experiments [11].

Parameter	Magnetopause [14, 16]	Sim. I	Sim. II	Exp. [11]
v_0 (km s^{-1})	100–200	300	300	300
n_0 (m^{-3})	$\approx 2 \times 10^7$	10^{15}	10^{16}	10^{18}
$B_\perp$ (T)	(10–30) $\times 10^{-9}$	0.05	0.05	0.015
$m_\mathrm{i}/m_\mathrm{e}$	1836	92	92	1836
$\beta_\mathrm{k} = W_\mathrm{K}/W_\mathrm{B}$	0.5–17	8×10^{-5}	8×10^{-4}	0.8
$W_\mathrm{K}/W_\mathrm{E}$	(0.4–4) $\times 10^7$	76	756	8×10^5
$\frac{1}{10}\frac{W_\mathrm{K}}{W_\mathrm{E}}\sqrt{\frac{m_\mathrm{e}}{m_\mathrm{i}}}$	(1–9) $\times 10^4$	0.79	7.9	2×10^3
$\Pi = \frac{w}{r_\mathrm{gi}} K \sqrt{\beta_\mathrm{ith}}$		1.3×10^{-3}	4.2×10^{-3}	0.1
f_pe	40 kHz	63 MHz	200 MHz	9 GHz
f_ce	(0.3–0.8) kHz	70 MHz	70 MHz	0.4 GHz
f_pi	0.9 kHz	7 MHz	20 MHz	0.2 GHz
f_lh	(7–20) Hz	5 MHz	7 MHz	10 MHz

where $\hat{\boldsymbol{y}}$ and $\hat{\boldsymbol{z}}$ are unit vectors in the y- and z-directions, respectively. For this simulation, $B_0 = 0.05\,\mathrm{T}$ is the horizontal component of the magnetic field, $z_\mathrm{T} = 165\,\mathrm{mm}$ is the z-coordinate of the centre of the transition region and $\delta = 20\,\mathrm{mm}$ is a constant that determines how sharp the magnetic field gradient will be.

Initially the plasma is uniform within a cylinder of length $L = 110\,\mathrm{mm}$ and radius $R = 12.5\,\mathrm{mm}$. The plasmoid width $w = 2R = 25\,\mathrm{mm}$ is thus smaller than the ion gyro-radius $r_\mathrm{gi} = m_\mathrm{i} v_0/(\mathrm{e}B_0) = 63\,\mathrm{mm}$ but larger than the electron gyro-radius $r_\mathrm{ge} = 0.68\,\mathrm{mm}$. The plasma cylinder is centred at $(x_0, y_0, z_0) = (22.5, 32.5, 80)\,\mathrm{mm}$. The size of the simulation box is $(L_x, L_y, L_z) = (45, 65, 150)\,\mathrm{mm}$. In this paper we present two simulation runs. In simulation I, the initial density is $10^{15}\,\mathrm{m}^{-3}$ and in simulation II, $n_0 = 10^{16}\,\mathrm{m}^{-3}$. We simulate 560 ns in both cases with a time step of $\Delta t = 0.8\,\mathrm{ns}$ in simulation I and $\Delta t = 0.4\,\mathrm{ns}$ in simulation II. Some important parameters for the two simulation runs are shown in table 1 together with typical parameters from the laboratory [11] and the magnetopause [14, 16].

In the experiments, lower-hybrid waves were observed and these were interpreted as resulting from a modified two-stream instability [7]. One would then have a maximum growth rate of $\gamma_\mathrm{max} = \omega_\mathrm{lh}/2$ at wave number $k_\mathrm{max} = \sqrt{3}\omega_\mathrm{lh}/v_\mathrm{ei}$ [17], where $\omega_\mathrm{lh} = 2\pi f_\mathrm{lh} = 2\pi f_\mathrm{pi}\sqrt{1 + f_\mathrm{pe}^2/f_\mathrm{ce}^2}$ is the lower-hybrid frequency, and $v_\mathrm{ei} = i/(n\mathrm{e})$ is the relative electron–ion drift speed associated with the current across $\boldsymbol{B}$ that drives the instability. In the experiment of Hurtig *et al* [7, 8], v_ei was typically $10^5\,\mathrm{m\,s^{-1}}$, about one-third of the plasma speed, $v_0 = 3 \times 10^5\,\mathrm{m\,s^{-1}}$. Assuming the same velocity ratio, and the parameters used in the simulations that are reported here, the wavelengths of maximum growth would be 1.2 cm and 0.8 cm in simulations I and II, respectively.

The frequency for the fastest growing mode would be $\sqrt{3}f_\mathrm{lh}/2$. Thus, with parameters from table 1, we can fit several wavelengths inside the simulated plasma, and the simulation is run for a few growth times and wave periods. The experimental parameters, in the rightmost column of table 1, would require both a spatial and a temporal resolution that would be computationally prohibitive. With the parameters that we do use, we can, however, demonstrate the ability to study the wave growth by simulating a parameter regime that previously had not been simulated. The present simulations have been motivated by a renewed effort in laboratory experiments, the advances in computer performance, and by spacecraft missions utilizing simultaneous measurements at several points in space.

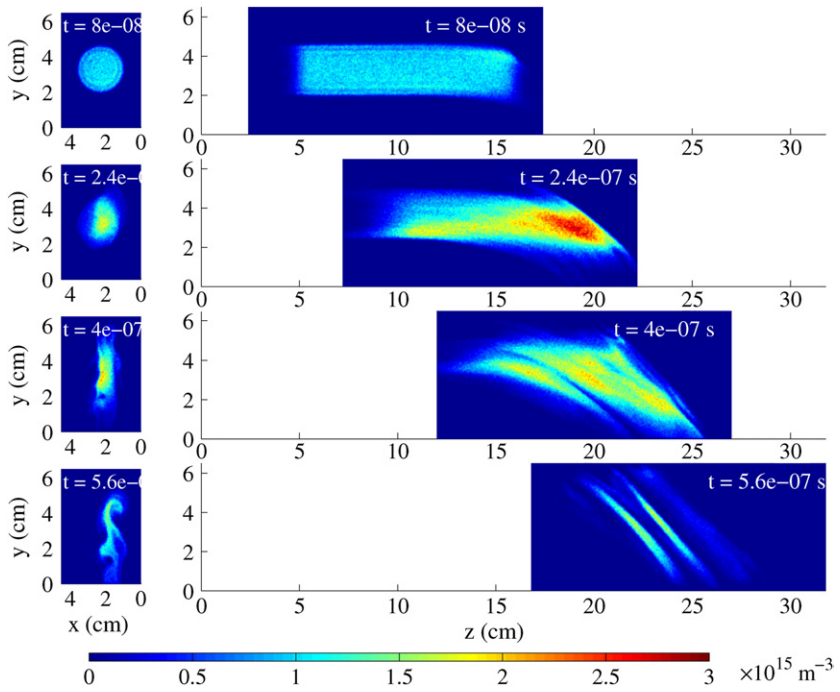

Figure 2. Slices of the electron density in the xy-plane (left column) and the yz-plane (right column) for the times $t = 80$, 240, 400 and 560 ns in simulation I. These times correspond to $tf_{\mathrm{lh}} = 0.39$, 1.2, 2.0, and 2.7.

3. Simulation results

Figure 2 shows the plasma density of simulation I in the xy-plane (left column) and the yz-plane (right column) for the times $t = 80$, 240, 400 and 560 ns from top to bottom. Figure 3 shows the same thing for simulation II. The coordinate perpendicular to the plane shown in each panel is at the centre of the original plasma cylinder.

As the plasma enters the transverse field region, it is compressed in the x-direction, which is perpendicular both to its motion and to the magnetic field, in agreement with laboratory experiments [5, 11]. The compression was explained by Hurtig *et al* [11] as a result of the $\boldsymbol{j} \times \boldsymbol{B}$-force arising from the diamagnetic current. Density structures that are aligned with the $\boldsymbol{B}$-field appear in and after the transition region. Comparing the lower panels of figures 2 and 3, one can see that, at the end of the run, the lower-density plasma of simulation I has slowed down more, and penetrated less, than the higher-density plasma of simulation II.

The upper panel of figure 4 shows the density in simulation I as it would be measured by a probe located at $(x, y, z) = (25, 32.5, 210)$ mm. The x-coordinate of the probe is shifted 2.5 mm from the centre of the plasma ($x_0 = 22.5$ mm) towards the high potential side. The lower panel shows the power spectral density P_{nn} of $n_{\mathrm{p}} - \langle n_{\mathrm{p}} \rangle$, where n_{p} is the density measured by the probe and $\langle n_{\mathrm{p}} \rangle$ is the mean value of the density during the time shown in the upper panel. The power spectral density was computed using Welch's method which, for example, is described in [18], with a Hanning window and 65% overlap. The corresponding quantities in simulation II are shown in figure 5. The strong wave activity can be seen in the probe signal near the end of the trace. This is similar to what was observed experimentally by Hurtig *et al* [7]. The wave frequency is in the lower-hybrid range in both simulations. In simulation I, where

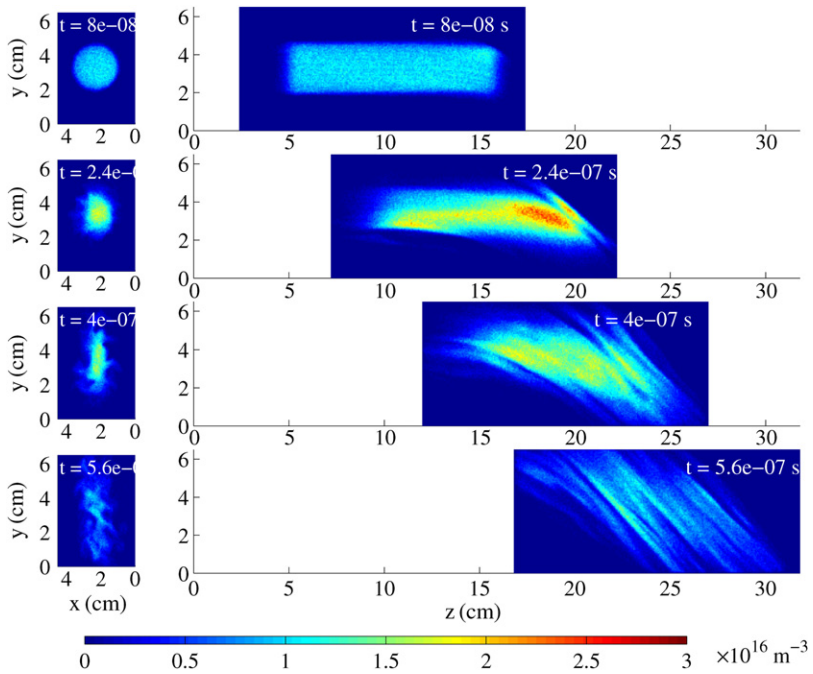

Figure 3. Slices of the electron density in the xy-plane (left column) and the yz-plane (right column) for the times $t = 80$, 240, 400 and 560 ns in simulation II. These times correspond to $tf_{\mathrm{lh}} = 0.55$, 1.7, 2.8 and 3.9.

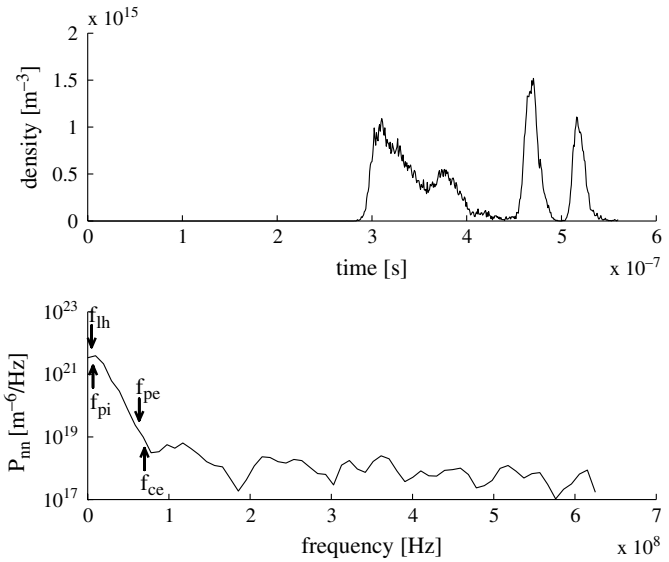

Figure 4. The upper panel shows the signal from a density-measuring virtual probe located at $x = 25$ mm, $y = 32.5$ mm, $z = 210$ mm in simulation I. The probe location is 2.5 mm to the high potential side of the centre of the plasma. The lower panel shows the power spectral density of this signal after subtraction of its mean value. The lower-hybrid frequency, the ion and electron plasma frequencies, and electron cyclotron frequency are marked using arrows in the lower panel.

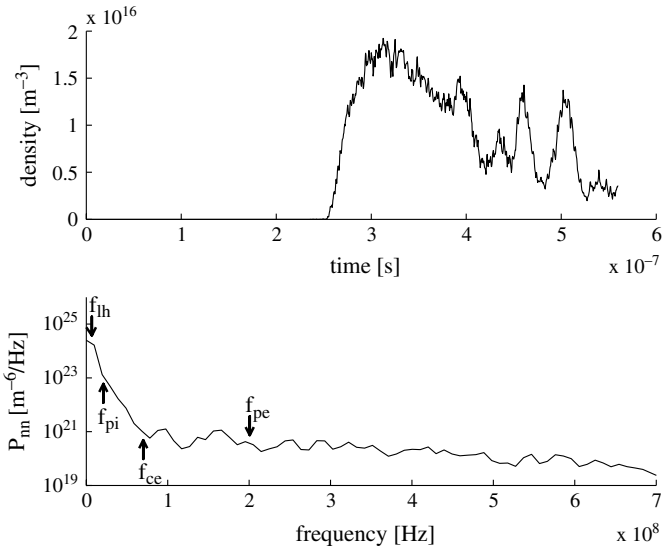

Figure 5. The upper panel shows the signal from a density-measuring virtual probe located at $x = 25$ mm, $y = 32.5$ mm, $z = 210$ mm in simulation II. The probe location is 2.5 mm to the high potential side of the centre of the plasma. The lower panel shows the power spectral density of this signal after subtraction of its mean value. The lower-hybrid frequency, the ion and electron plasma frequencies, and electron cyclotron frequency are marked using arrows in the lower panel.

the density is lower, the lower-hybrid frequency cannot be distinguished from the ion plasma frequency. In simulation I, the density is 100% modulated, all the way down to zero, and, in simulation II, the oscillation amplitude is a large fraction of the background density. This is consistent with the experimental findings [7]. It should be noted that the density structures in figures 4 and 5 correspond to observations in the lab frame. These frequencies are Doppler up-shifted from those that would be seen in the plasma rest frame. An exact identification with the lower-hybrid frequency is therefore not expected. The central finding is that the oscillations are in the lower-hybrid range.

Space–time diagrams of the plasma density for the x- and y-coordinates are shown in figure 6 for simulation I and in figure 7 for simulation II. There are waves propagating in the y-direction with a phase speed of 250–300 km s^{-1} in both simulations, that is to say, at about the bulk speed of the plasma. In z–t-diagrams (not shown) one can see that the phase speed in the z-direction is in the same range as that in the y-direction.

As determined from the data in figures 6 and 7 and from the lower right-hand panels in figures 2 and 3, the dominating wavelength in simulation I is $\lambda_y \approx 1.3$ cm and $\lambda_z \approx 1.5$ cm, and, in simulation II, $\lambda_y \approx 1.4$ cm and $\lambda_z \approx 0.7$ cm. Careful examination of the right-hand panel of figure 7 indicates the presence of smaller amplitude structure with λ_y in the vicinity of the 0.7 cm determined for λ_z. This means that, in simulation II, there is a spectrum of several wavelengths, whereas, in simulation I, there is one clearly dominating wavelength. This can also be discerned from a comparison of the lower right ($t = 560$ ns) panels of figures 2 and 3.

4. Implications for space studies

Whether or not a plasmoid will penetrate the magnetopause on impact depends on its values of β_k and Π [15]. The nature of the penetration also depends on these quantities.

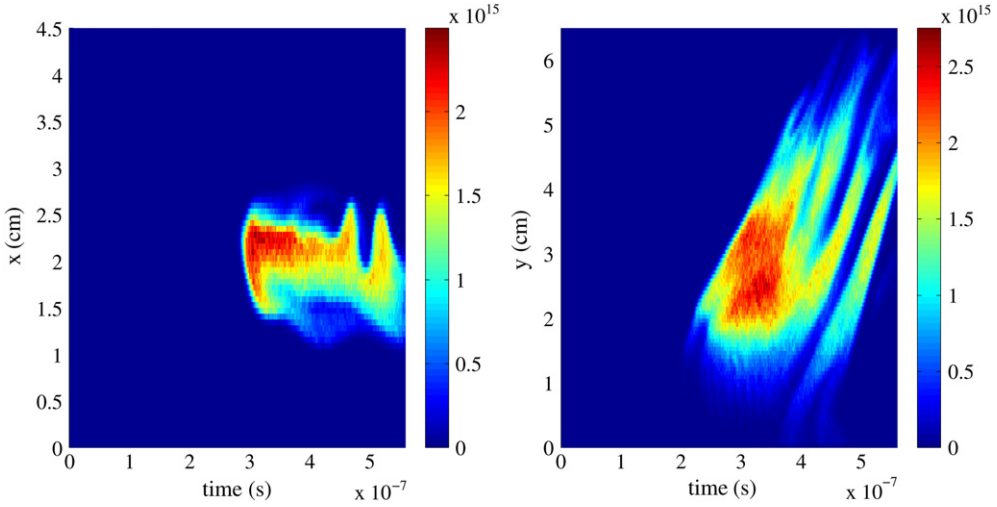

Figure 6. x–t- and y–t-diagrams for the density at $z = 0.21$ m in simulation I.

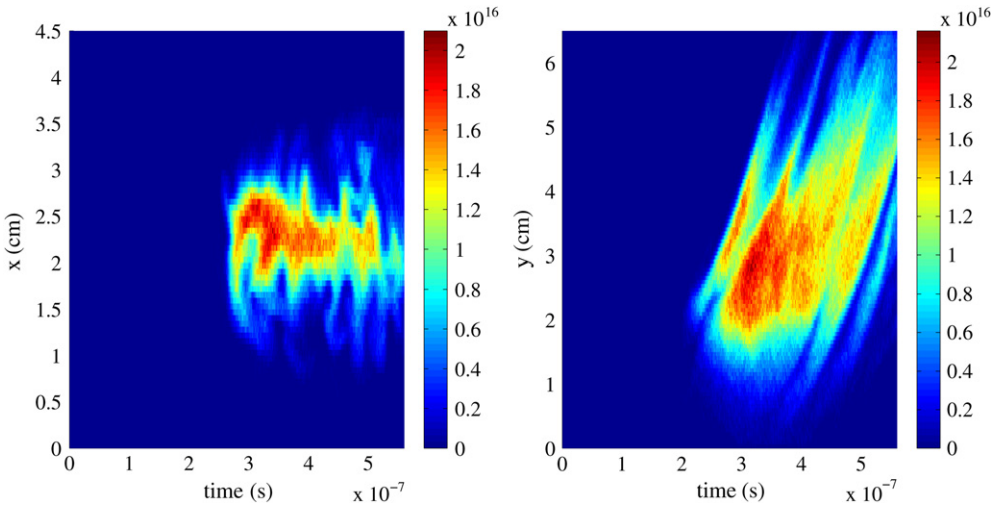

Figure 7. x–t- and y–t-diagrams for the density at $z = 0.21$ m in simulation II.

A multi-spacecraft approach to measure the size of the plasmoids is necessary for our understanding of the physics involved because the width of the plasmoid is one of the quantities that determine what type of model can describe the penetration.

An estimate of the upper limit to the width of a plasmoid that can penetrate through self-polarization can be made using the inequalities in section 1 [15], parameters from table 1 and $k_B T_i = 200\,\mathrm{eV}$ [16]. For $v_0 = 100\,\mathrm{km\,s^{-1}}$ and $B = 30\,\mathrm{nT}$ this leads to $w \approx 8\,\mathrm{km} \approx 0.2 r_{gi}$. For $v_0 = 200\,\mathrm{km\,s^{-1}}$ and $B = 10\,\mathrm{nT}$ we obtain $w \approx 93\,\mathrm{km} \approx 0.4 r_{gi}$, where r_{gi} is the drift speed gyro-radius. In the magnetosheath, on the other hand, they gyrate at their thermal speed, leading to $w \approx 0.6 r_{gi}$ before penetration, which must still be considered as small. A structure that is small enough to penetrate the magnetopause through self-polarization would need to be created at or near the magnetopause, since it otherwise would soon disperse and grow to sizes

of at least one gyro-diameter. The sideways contraction, by a factor 3–5, seen in the left-hand panels of figures 2 and 3 would simplify penetration of clouds that are initially too wide. Also, as we have seen in section 3, lower-hybrid waves can create small scale density structures and lower-hybrid waves have been observed at the magnetopause [14]. The understanding of the physics of magnetopause penetration in the self-polarization regime thus requires not only a search for small plasmoids, but also that wave processes at the magnetopause are studied. Unfortunately, we are unable to reach the β_k of the magnetopause in our simulations as can be seen in table 1. However, waves on the lower-hybrid frequency scale are seen both in the simulations presented here and in laboratory experiments. These simulations can therefore model wave phenomena in the electrostatic regime of the experiments. The β_k parameter of the laboratory experiment is in the range of values seen at the magnetopause, and therefore wave phenomena of the kind reported here are expected at the magnetopause for the small plasmoid conditions that are described above.

Lindberg [5] pointed out that the polarization field builds up a potential which the ions must overcome. He found that this sets an upper limit to the width of the penetrating plasmoid:

$$w \leqslant \frac{1}{2}\frac{m_i v_0}{eB_y} = \frac{1}{2} r_{gi}. \tag{3}$$

Here $B_y = B_\perp$ downstream and $B_y = 0$ upstream of the barrier. Since the solar wind is magnetized, this condition is modified at the magnetopause, where the upstream B_y may differ from zero. With the experimental coordinate system used throughout this paper, i.e. the downstream magnetic field $\boldsymbol{B}_d = B_{yd}\hat{\boldsymbol{y}}$, with the upstream field $\boldsymbol{B}_u = B_{xu}\hat{\boldsymbol{x}} + B_{yu}\hat{\boldsymbol{y}} + B_{zu}\hat{\boldsymbol{z}}$, and with $\boldsymbol{v}_0 = v_0\hat{\boldsymbol{z}}$, we have

$$ew(-\boldsymbol{v}_0 \times \boldsymbol{B}_d - (-\boldsymbol{v}_0 \times \boldsymbol{B}_u)) \cdot \hat{\boldsymbol{x}} = ewv_0(B_{yd} - B_{yu}) \leqslant \frac{m_i v_0^2}{2}. \tag{4}$$

From (4) we obtain the following plasmoid-width condition.

$$w \leqslant \frac{1}{2} r_{gi} \frac{B_{yd}}{B_{yd} - B_{yu}}. \tag{5}$$

If $B_{yu} = B_{yd}$, there is no barrier and, if $B_{yu} = 0$, we retain Lindberg's limit. If B_{yu} and B_{yd} are anti-parallel, the potential that must be overcome by the ions will be higher and the restriction on w more severe. It has been shown [15] that (3) is not an absolute requirement since wave processes can act so that the ions need not lose all their kinetic energy while entering the high potential region: on an average, the streaks with high density in the wave structure are associated with a wave electric field along the stream direction, and the voids in between with a wave field in the opposite direction. Even though conditions (3) and hence (5) need not necessarily be fulfilled, the ions must climb a potential hill to reach the high potential side and the direction of the upstream magnetic field will influence this process.

As can be seen from (4) and (5), the conditions are more favourable for penetration when the magnetic fields on both sides of the barrier are parallel. For penetration of the magnetopause this situation occurs when the interplanetary magnetic field (IMF) has a northward component. By searching space data, for example data from the Cluster spacecraft, from periods with a northward IMF penetrating plasmoids are more likely to be found. The magnetic field configuration with a northward IMF is also less favourable for reconnection, in the absence of anti-parallel magnetic fields, and that will make the identification of impulsive penetration events easier.

5. Discussion

In impulsive penetration, plasma can penetrate a magnetic barrier without magnetic reconnection, i.e. without rearranging of the magnetic field topology. Both processes require collisionless resistivity both to enable electron diffusion and to dissipate magnetic energy. Experiments have shown that waves in the lower-hybrid frequency range can provide the required resistivity [8]. The simulations presented here reproduce these waves but, due to computational limitations, we can accommodate only a couple of wave periods near the end of the simulations (see figures 4 and 5) and we do not have good enough statistics to reliably compute the resistivity.

There are two processes: impulsive penetration and reconnection. They both require a collisionless resistivity, and we have seen that this can be provided by waves. What distinguishes the two? One may speculate that the microphysics is similar in the two cases and that reconnection occurs when the magnetic field topology is such that it can be rearranged by dissipation of magnetic energy in a diffusion region. At the magnetopause this is most likely during periods with southward IMF. During northward IMF the magnetic field topology cannot be rearranged in this way and impulsive penetration happens instead. Laboratory experiments can be used to study both the regimes of self-polarization and of magnetic expulsion in considerable detail [8]. Only one experiment [6] has been made, so far, of the transition to the rejection regime, which, after all, should be the normal state at the magnetopause. We have presented three-dimensional electrostatic simulations. These are applicable to the self-polarization regime, and shall be used in future studies of the transition to the rejection regime. Thus they can be used to model a subset of the laboratory experiments and penetration of the magnetopause for plasmoids that are small enough to penetrate through self-polarization. To accurately model the magnetic expulsion regime, one would need to rely on electromagnetic simulations. Future work should include a combination of space, laboratory and simulation studies. The relationship between impulsive penetration and magnetic reconnection can be studied by comparing these results with results from reconnection experiments with colliding magnetized plasmas (see review by Yamada [19]). Space observations can be used both to find penetrating plasmoids and to measure their size. Multi-point measurements, for example with the Cluster spacecraft, would be crucial in this context. Detailed observations of waves at the magnetopause that can be compared with results from the laboratory and computer simulations would greatly increase our understanding of the processes involved.

Acknowledgments

This work was supported by the US Department of Energy (DE-FG02-06ER46267), the US National Science Foundation (NSF-PHYS-0613238) and the Swedish National Space Board.

References

[1] Lemaire J 1977 Impulsive penetration of filamentary plasma elements into the magnetospheres of the earth and jupiter *Planet. Space Sci.* **25** 887–90

[2] Carlson C W and Torbert R B 1980 Solar wind ion injections in the morning auroral oval *J. Geophys. Res.* **85** 2903–8

[3] Woch J and Lundin R 1992 Signatures of transient boundary layer processes observed with Viking *J. Geophys. Res.* **97** 1431–47

[4] Lundin R *et al* 2003 Evidence for impulsive solar wind plasma penetration through the dayside magnetopause *Ann. Geophys.* **21** 457–72

[5] Lindberg L 1978 Plasma flow in a curved magnetic field *Astrophys. Space Sci.* **55** 203–25

[6] Ishizuka H and Robertson S 1982 Propagation of an intense charge-neutralized ion beam transverse to a magnetic field *Phys. Fluids* **25** 2353–8
[7] Hurtig T, Brenning N and Raadu M A 2004 The penetration of plasma clouds across magnetic boundaries: the role of high frequency oscillations *Phys. Plasmas* **11** L33–6
[8] Hurtig T, Brenning N and Raadu M A 2005 The role of high frequency oscillations in the penetration of plasma clouds across magnetic boundaries *Phys. Plasmas* **12** 012308
[9] Echim M M and Lemaire J F 2000 Laboratory and numerical simulations of the impulsive penetration mechanism *Space Sci. Rev.* **92** 565–601
[10] Echim M M, Lemaire J F and Roth M 2005 Self-consistent solution for a collisionless plasma slab in motion across a magnetic field *Phys. Plasmas* **12** 072904
[11] Hurtig T, Brenning N and Raadu M A 2003 Three-dimensional electrostatic particle-in-cell simulation with open boundaries applied to a plasma beam entering a curved magnetic field *Phys. Plasmas* **10** 4291–305
[12] Schmidt G 1960 Plasma motion across magnetic fields *Phys. Fluids* **3** 961–5
[13] Peter W and Rostoker N 1982 Theory of plasma injection into a magnetic field *Phys. Fluids* **25** 730–5
[14] André M *et al* 2001 Multi-spacecraft observations of broadband waves near the lower hybrid frequency at the earthward edge of the magnetopause *Ann. Geophys.* **19** 1471–81
[15] Brenning N, Hurtig T and Raadu M A 2005 Conditions for plasmoid penetration across abrupt magnetic barriers *Phys. Plasmas* **12** 012309
[16] Sundkvist D, Retinò A, Vaivads A and Bale S D 2007 Dissipation in turbulent plasma due to reconnection in thin current sheets *Phys. Rev. Lett.* **99** 025004
[17] McBride J B, Ott E, Boris J P and Owens J H 1972 Theory and simulation of turbulent heating by the modified two-stream instability *Phys. Fluids* **15** 2367–83
[18] Stoica P and Moses R L 1997 *Introduction to Spectral Analysis* (Upper Saddle River, NJ: Prentice-Hall)
[19] Yamada M 1999 Review of controlled laboratory experiments on physics of magnetic reconnection *J. Geophys. Res.* **104** 14529–42